Chapter 1

Introduction

One of the driving forces behind our modern society is the phenomenon of catalysis. Catalysts are, for instance, applied in the pharmaceutical industry and petrochemical industry to produce clean and specific products. Another important application is the field of pollution control, for example to reduce the emission of hazardous gases from vehicles and power plants. The development of the modern use of catalysts was initiated in the early nineteenth century by Kirchhoff, H. Davy, E. Davy, Döbereiner and Faraday, who were the first ones to study this phenomenon, in which chemical reactions were aided by the presence of other materials, which were not consumed in the process. Twenty years after its initial reporting, it was Berzelius who in 1836 named this phenomenon as "catalysis" [1]. The second half of the nineteenth century was filled with discoveries, and the development of numerous catalysis based reaction systems; an example is the Deacon process (1860), in which Cl_2 was produced from HCl, over a $CuCl_2$ catalyst [2, 3]. The first big industrialized and researched catalytic system was for the synthesis of NH_3, an important basic ingredient for making fertilizers. The research led, in particular, to the introduction of high-pressure reactors, in order to shift the chemical equilibrium of the NH_3 synthesis reaction towards higher product yield. During the same period, science became involved in catalysis, and began studying, for instance, the active sites of a catalyst, the sticking probability of molecules on a catalyst surface, and the kinetic mechanisms of catalytic systems. The increasing use of fuel during the twentieth century, and consciousness about the necessity of controlling the composition of the gases emitted into the atmosphere, to decrease our impact on the environment, have led to the exponential development of catalysts, as well as the development of the research field of catalysis worldwide. To emphasize the importance of this research field, Gerhard Ertl was awarded the Nobel Prize in chemistry in 2007, for his work in this field [4].

The work I present in my thesis adds knowledge and interpretation to a subsection of the wonderful and indispensable phenomenon of catalysis. This first chapter gives an overview of the theory behind catalysts, the different research techniques which engage our increasing fundamental understanding of catalysts, a short introduction to crystallography, as well as the ins and outs of the specific technique I used (Scanning Tunneling Microscopy (STM)) during my research.

1.1 Catalysts: theory and experiment

1.1.1 Catalysis

A catalyst is defined as a material which is directly and actively involved in accelerating a selected chemical reaction, without being consumed itself. It can accelerate a chemical reaction by lowering the activation energies involved in this reaction, which is schematically shown in figure 1.1. The catalyst can lower the activation energy by providing alternate pathways for a reaction to take place, e.g. by enabling adsorption, diffusion, and chemical rearrangements of reactants, and desorption of the reaction products. Next to just accelerating a reaction, the catalyst also has to be selective, i.e. it should only lower the energy barriers for the desired reaction to occur.

Catalysis can be divided in two categories: homogeneous and heterogeneous catalysis. In the former case, both the catalyst and the reactants are in the same phase. Examples of this type of catalysis are the hydroformylation of alkenes into aldehydes, which are an important basic product for many detergents (liquid phase) [7], and the decomposition of ozone in the atmosphere by halogenoid radicals (gas phase) [8]. Yet the vast majority of catalyzed reactions fall within the scope of heterogeneous catalysis, in which reactants and catalyst are in different phases. In most heterogeneously catalyzed reactions, liquid or gaseous reactants react on the surface of a solid catalyst. Therefore, the key to understanding how heterogeneous catalysis works is to understand how the surface behaves, under the presence of the reactants, at pressure p and temperature T. The reactivity of a catalyst scales directly with the number of active sites, and since many of the catalyst materials consist of precious transition metals, in industry the catalysts generally are dispersed as nano-particles on a porous grid, made out of a cheap support material (e.g. Al_2O_3), in order to optimize the surface-to-volume ratio. The production of plastics, medicines, and fuels are well-known examples

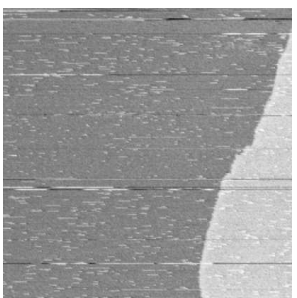

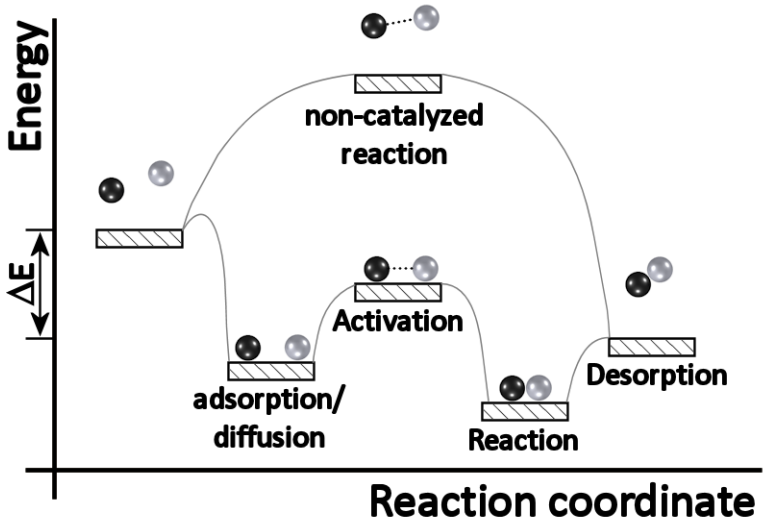

Figure 1.1: Schematic energy diagram for a catalyzed and non-catalyzed reaction. ΔE is the energy gained by the total reaction.

of heterogeneous catalysis; this work consists solely of heterogenic catalytic systems.

The main field of catalysis, on which this thesis is built, is the field of minimizing our environmental impact, while combusting fuels in transportation. This can be approached from two directions. The *ingoing* fuel can be cleaned as well as possible by, for instance, catalytic removal of sulfur (chapter 5) and nitrogen from carbon hydrates containing these elements. Catalytic removal of hazardous gases from the *outgoing* exhaust gas composition, after the fuel has been combusted in the engine, is the other option. The typical gas composition, from the exhaust of a spark ignition engine in a car, consists of three types of compounds: (1) oxidant chemical compounds (O_2, NO_x), (2) reducing chemical compounds (CO, H_2, unburnt hydrocarbons), and (3) other compounds (N_2, H_2O, CO_2) [9]. The three-way catalyst of a car exploits three reactions: NO_x reduction (chapter 3), CO oxidation (chapter 4), and oxidation of unburnt hydrocarbons.

1.1.2 Langmuir theory of adsorption

During a catalyzed chemical reaction, one or more of the reactants form a bond to the surface of the catalyst by a process called adsorption. There are two kinds of adsorption: associative and dissociative adsorption. For the

latter, the adsorbate molecule splits when bonded to the surface, whereas for associative adsorption, it does not. The theory of gases adsorbed on a solid surface at equilibrium can be described by the Langmuir theorem of adsorption. In this theory, a combination of assumptions has been made:

- The solid surface is uniform, and consists of equivalent sites, which can be occupied by only one gas molecule.
- The equilibrium between the gas and adsorbate state is dynamic.
- When a gas molecule collides with the surface and hits an empty site, it is bonded; otherwise it is reflected.
- Adsorbed molecules are localized.

The fractional coverage of the surface ϑ depends on the number of occupied sites N_S and the total number of sites N: $\vartheta = \frac{N_S}{N}$. Since in our experiments, we control the fractional coverage of gas M by altering the pressure of the gas offered to the surface, it is instructive to write the dependence of ϑ on the pressure p. For determining the fractional coverage of associative adsorption, we first write down its general reaction between surface and gas, $M_{(g)} + * \rightleftharpoons M_{(ads)}$. Here $*$ stands for a free site on the surface, and $M_{(ads)}$ is the complex of the adsorbed molecule and the site it occupies. From the reaction equation, we can determine the adsorption rate A and the desorption rate D: $A = k_a p(1-\vartheta)$, in which k_a is the adsorption rate constant and $(1-\vartheta)$ the relative density of free sites on the surface; $D = k_d\vartheta$, in which k_d is the desorption rate constant. At equilibrium $A = D$, so that $\vartheta(p)$ reads

$$\vartheta = \frac{Kp}{1+Kp}, \tag{1.1.1}$$

in which K is the equilibrium constant defined by $\frac{k_a}{k_d}$, and in this case can be interpreted as the affinity of the molecules for the surface: when K increases, k_a gets larger relative to k_d, implying that adsorption becomes more favorable than desorption. Equation 1.1.1 is called the Langmuir adsorption isotherm, and predicts how the fractional coverage changes with the pressure.

In the same way, the Langmuir adsorption isotherm for dissociative adsorption can be determined. Let us consider the example of a homonuclear, diatomic molecule M_2. In this case, the reaction equation is given by $M_{2\ (g)} + 2 * \rightleftharpoons 2\ M_{ads}$, yielding adsorption rate $A' = k'_a p(1-\vartheta)^2$ and desorption rate $D' = k'_d\vartheta^2$. Following the same calculation as for associative adsorption, the Langmuir dissociative adsorption isotherm becomes

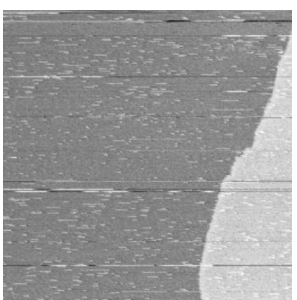

$$\vartheta = \frac{\sqrt{K'p}}{1+\sqrt{K'p}}. \tag{1.1.2}$$

At low pressures, $K^{(')}p \ll 1$, resulting in the linear expression $\vartheta(p) = K^{(')}p$, which is known as Henry's law. If we look at the extreme $p \to \infty$, we obtain $\vartheta = 1$, implying that at elevated pressures, which is our working domain, the solid surface will be completely covered by a monolayer of adsorbed gas molecules.

1.1.3 Reaction mechanisms

Investigations on adsorption and desorption of gas molecules at a catalytically active surface, and interaction of these molecules with each other on this surface, as well as with the surface itself, have yielded various reaction mechanisms. The main reaction mechanisms, two of which are also encountered in this work, are shown in figure 1.2.

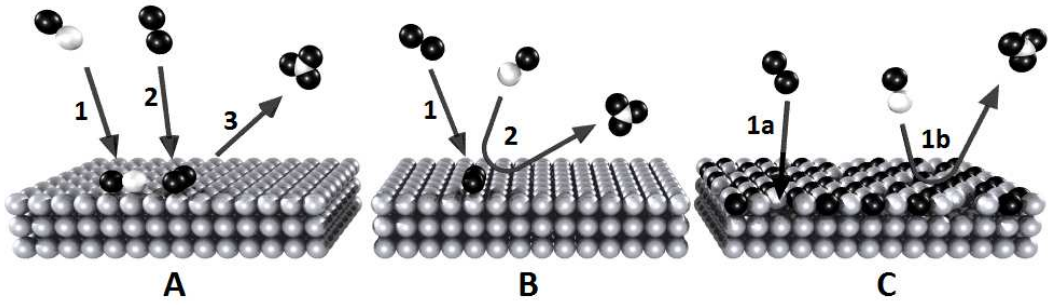

Figure 1.2: (A) Langmuir-Hinshelwood mechanism, (B) Eley-Rideal mechanism, (C) Mars-Van Krevelen mechanism

Part A in figure 1.2 shows the Langmuir-Hinshelwood mechanism. In this reaction mechanism, both reactants first adsorb onto the surface (reaction 1 and 2), before a reaction takes place. Surface diffusion facilitates interaction between adsorbed molecules; the reaction product desorbs from the surface (reaction 3). Generally, the reaction rate between adsorbent 1 and 2 is given by $R_{LH} = k\vartheta_1\vartheta_2$, provided that the reaction at the surface is the rate limiting step, in which k is the reaction constant. Its dependence on the pressure is given in equation 1.1.3, which is derived from the Langmuir adsorption isotherm derived in section 1.1.2.

$$R_{LH} = k\frac{K_1p_1 \cdot K_2p_2}{(1+K_1p_1+K_2p_2)^2}. \tag{1.1.3}$$

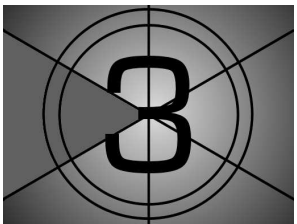

In this type of mechanism, the reactivity is highest when a stoichiometric amount of reactant is adsorbed on the surface, and both reactants are fully dispersed over the surface. The vast majority of catalytic reactions follow this mechanism. An example is the reduction of NO by CO on Pt(100), which is described in detail in chapter 3.

A second mechanism, the Eley-Rideal mechanism, is shown in part B of figure 1.2. In this case, only one of the reactants adsorbs onto the surface (reaction 1), after which the other reactant interacts with the adsorbed species directly from the gas phase, followed by the desorption of the reaction product (reaction 2). The reaction rate is therefore given by $R_{ER} = k\vartheta_1 p_2$, which translates to equation 1.1.4 if we substitute the Langmuir adsorption isotherm.

$$R_{ER} = k\frac{K_1 p_1}{1 + K_1 p_1} p_2. \tag{1.1.4}$$

A higher coverage of the adsorbed species, as well as a higher pressure of the other gas, yields a higher reaction rate. An example of a reaction following the Eley-Rideal mechanism is the hydrogenation of CO_2 during formate synthesis [25], in which H_2 is the adsorbed species.

Finally, in part C of figure 1.2, the Mars-Van Krevelen mechanism is depicted. In this mechanism, the surface itself is an active part in the reaction: one reactant forms a chemical bond with the catalytic surface (reaction 1a), forming a thin surface layer of Metal-Reactant. Examples are metal oxides, carbides, and sulfides. The other reactant now reacts directly from the gas phase with the atoms from the chemically bonded reactant on the surface (reaction 1b), yielding a reaction rate of $R_{MvK} = k\vartheta_{1a} p_{1b}$. This has the same mathematical form as Eley-Rideal kinetics. When the reaction product desorbs, a vacancy is left behind in the surface. This vacancy will be filled again by the first reactant (reaction 1a). In principle, in the mechanism as described by Mars and Van Krevelen in 1954 [26], the vacancy created by the reaction is filled by a reactant atom from the bulk, rather than the gas phase. In my view, however, it is purely a semantic discussion whether the supply of atoms filling the vacancies originate from the bulk or the gas phase, since this difference does not influence the relevant processes within the reaction mechanism. An example of the Mars-Van Krevelen reaction mechanism is CO-oxidation under high oxygen pressure on platinum – the surface forms a surface oxide with which the CO interacts [27]. In this particular case, roughening of the surface takes place; when an oxygen vacancy is created, the uncoordinated platinum atom becomes highly mobile, and starts diffusing

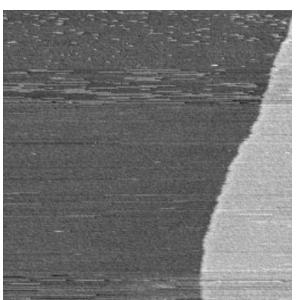

on the surface, until a reaction with an oxygen molecule from the gas phase fixes it to its position. Under certain conditions, this leads to spontaneous reaction oscillations [28].

1.1.4 The traditional surface science approach

Catalysts in real working conditions are very complex systems. Many factors determine the activity and selectivity of a catalyst. A large surface-to-volume ratio, and adding certain additives, increase its yield. Often high temperature and pressure conditions are necessary for maximum productivity. On the other hand, catalysts experience degradation. At high temperatures, dispersed catalytic nano-particles undergo sintering, and small pollutions within the reactants or byproducts of the reaction can poison the surface of a catalyst, by blocking the active sites. Many of the catalysts used nowadays have been developed by trial and error; however, the fundamental approach towards understanding heterogeneous catalysis became a major field in surface science. Traditionally, simplified model catalysts, such as single crystals polished in a certain orientation (section 1.2), are studied under ultrahigh vacuum (UHV) conditions. Numerous surface sensitive techniques have been developed for catalyst characterization at different levels, of which a few are mentioned here. Auger electron spectroscopy and X-ray photo spectroscopy can be used for chemical characterization. Scanning tunneling microscopy, atomic force microscopy, surface X-ray diffraction, scanning and transmission electron microscopy, and low energy electron diffraction can be used for characterization of the surface structure of the catalyst. Infrared spectroscopy and high-resolution electron energy loss spectroscopy provide information about the vibrational properties of the surface. For theoretical studies, density functional theory and Monte Carlo simulations are common methods. Most of these surface sensitive techniques actually require the use of UHV. In order for information carriers such as ions, electrons, and photons to interact with the surface of a crystal, rather then the bulk, their energy should be low. To maintain a long mean free path for these low-energy carriers, they should not interact with gaseous molecules between source, substrate, and detector, hence the necessity for UHV. Moreover, the UHV provided a clean and well controllable environment for performing experiments [5, 6]. This approach has two substantial shortcomings, since catalysts in industry mostly consist of alloyed nano-particles, dispersed on a highly porous support material exposed to high pressures of reactants. These shortcomings are defined as the “pressure gap” and the “materials gap”, which will be discussed more thoroughly in the next section. Despite these disadvantages, these techniques did contribute substantially to our fundamental understanding of catalysts,

giving insights into the functioning of catalysts at the atomic level, the influence of steps, kinks, dangling bonds, uncoordinated atoms and surface dynamics, reaction mechanisms, and catalyst degradation mechanisms.

1.1.5 Gaps

The Pressure Gap

As mentioned in the previous section, surface sensitive techniques often require ultrahigh vacuum conditions, whereas, in industrial catalysis, high pressures are common. Recent investigations at high gas pressures have yielded knowledge which could not be predicted by extrapolating the low-pressure results [27, 36, 47, 48]. This discrepancy between science and industry is called the pressure gap [49, 50]. To illustrate the effect of a gas on the surface free energy γ, we define in equation 1.1.5 the Gibbs model, which states that the interface between two bulk phases, with a uniform concentration, can be seen as a surface of zero thickness, the Gibbs dividing surface. This surface describes the real system by accounting for the excess entropy, energies, and material [24].

$$\gamma = f^s - \sum_i \mu_i \Gamma_i. \tag{1.1.5}$$

In this equation, f^s is the Helmholtz free energy for the Gibbs dividing surface per unit area, while the sum describes the contribution of gas i by its chemical potential μ_i. Γ_i is the adsorption of component i. The chemical potential of gas i is given by equation 1.1.6, from which can be seen that it depends on the gas partial pressure p_i and the temperature T. μ_i^0 and p_i^0 are its reference potential and pressure; k_b is the Boltzmann constant.

$$\mu_i = \left(\frac{\partial F}{\partial n_i}\right)_{T,V,n_j} = \mu_i^0 + k_b T \ln \frac{p_i}{p_i^0}. \tag{1.1.6}$$

Via equation 1.1.6, we can now estimate the difference between the contributions of the gas to the surface free energy, when working in UHV or at ambient pressure. In comparison with adsorption experiments performed in UHV, with typically $p \approx 10^{-9}$ bar, the pressure is 9 orders of magnitude higher at ambient pressure, so the extra contribution per gas molecule, will be $9 \cdot 2.35kT \approx 0.54$ eV at room temperature, which irrefutably is a significant contribution to the surface free energy. One could argue that the same effect, of the chemical potential on the surface free energy, can be achieved by decreasing the temperature, instead of increasing the pressure, meaning that in terms of thermodynamics, the situation with high (T,p) is equal to

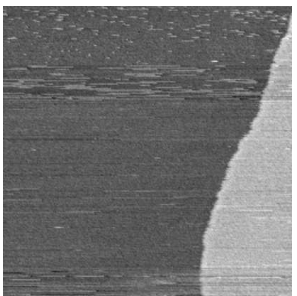

low (T,p) – so why push surface science techniques to the limit, by exposing them to extreme environments, if you can make life much simpler by cooling down your sample in ultrahigh vacuum? The answer to that question is catalytic activity. At a very low temperature, the surface of the catalyst will not be active at all, since the activation energies for separate reaction steps will be too high for them to occur at the surface in that situation. Another argument is the smearing of phase boundaries, between different surface terminations, under realistic conditions, as has been shown by kinetic Monte Carlo simulations [29]. At low (T,p), these boundaries will remain sharp. At present, much effort is being made to overcome both the materials and the pressure gaps, as will be described in more detail in chapter 2.

As an example of a pressure gap effect, a theoretical study, consisting of a constraint thermodynamics study, in combination with kinetic Monte Carlo simulations [29, 30] on CO oxidation on Pd(100), has shown that, under relevant reactant feed conditions, i.e. a stoichiometric supply of CO and O_2 at ambient pressures, the most stable phase is a surface oxide. However, this situation is close to a phase boundary, with a CO-covered metallic Pd(100) surface. Slight variations in temperature and pressure can easily shift the equilibrium across this phase boundary, initiating a phase transition. This means that coexistence of surface oxide patches and CO-covered metallic patches are plausible, even under steady state conditions. Oscillations in this situation are conceivable, so in order to understand the whole catalytic system, both phases, and the transition between these phases, have to be studied under ambient conditions.

The Materials Gap

A second drawback, the materials gap, was mentioned in section 1.1.4, next to the pressure gap. Industrial catalysts often consist of metal alloys dispersed as nano-particles on oxides. Additionally, the catalyst is usually enriched by promoters to increase its yield. The two main reasons to disperse catalysts as nano-particles are firstly, the maximization of the available active sites for the reaction, and secondly, the reduction of the amount of catalyst material needed, since many of the catalytically active transition metals are expensive. These complex cocktails of materials are too complicated to study with surface science techniques, which necessitates simple model systems, often in the form of bulk single crystals. The following differences between industry and science arise from this simplification step. Step, edge, and kink sites contribute significantly to the surface area of nano-particles. On single crys-

tals, the number of these types of sites is relatively small, which can cause a strong decrease in activity. Moreover, the boundary between support material and catalyst, and between various facets on catalyst nano-particles, influence the electronic structure, and therefore the activity towards certain reactions. When using a single crystal surface, these interactions are totally absent. Furthermore, the activity of a catalyst can be strongly size-dependent, as for instance is the case with gold – bulk gold is inert, whereas gold nano-particles exhibit high catalytic activity [31–33]. The materials gap comprises these differences between real catalysts used in industry and model catalysts used in research.

1.1.6 Suitable techniques for realistic conditions

In the present study, different surface analysis techniques have been adapted to operate under realistic conditions. Examples, which will be briefly discussed in this section, are infrared reflection adsorption spectroscopy (IRAS) [34], X-ray photoemission spectroscopy (XPS) [45, 46], transmission electron microscopy (TEM) [51], surface X-ray diffraction (SXRD), [52], scanning tunneling microscopy (STM) [50, 53, 54], and atomic force microscopy (AFM) [55]. Of course, theory should also be mentioned here, since methods including density functional theory and kinetic Monte Carlo simulations provide considerable insight into the operation of catalysts in realistic conditions, and create a basis on which new experiments can be planned and the experimental results obtained can be explained.

In situ IRAS, under reaction conditions, has been facilitated by the construction of a high-pressure micro-cell, with CaF_2 walls. These are transparent for infrared light, and have been integrated in an ultrahigh vacuum system [34, 35]. IRAS is a technique, which can distinguish between different molecules adsorbed on a surface, by the vibrational characteristics of the bonds in each molecule. For characterizing catalytic reactions, this technique can be valuable: concentrations of reactants and reaction products can be measured, from which turn-over frequencies and reactivity of a catalytic sample can be determined. The major drawbacks of IRAS are its insensitivity to the surface and its insensitivity to metal-adsorbate bonds, since the vibrational frequencies of metal-adsorbate bonds are often lower (< 600 cm^{-1}) than the operational frequency range of IRAS.

X-ray photoemission spectroscopy is a very powerful technique in catalysis, because of its surface sensitivity. The surface elemental composition can be determined by core-level peak intensities, while a shift in these intensities

provides information about the chemical bonds at the surface. Traditionally, this technique had been limited to ultrahigh vacuum conditions, because of scattering of the emitted photoelectrons in the gas phase. The development of a differentially pumped electrostatic lens system enables this technique to operate under relatively high pressures, up to 5 mbar [45, 46]. This number also illustrates one of its disadvantages: although a huge step, from UHV to the millibar range, has been made, the technique cannot (yet) operate under realistic conditions.

Nano-reactors, which fit into the tip of a standard TEM, are under development, to realize in situ TEM studies at ambient conditions, including heterogeneous catalysis. This particular field in TEM is called environmental TEM (ETEM). The nano-reactors are based on MEMS[1] technology, and their windows are (1) electron transparent, and (2) placed very close to each other, in order to minimize the loss of intensity of the electron beam within the nano-reactor. Using the nano-reactors, it is possible, for example, to study the properties of catalytic nano-crystals on oxide supports, under reaction conditions. At the moment of writing, carbon contamination of the reactors is a major issue: the windows of the nano-reactors can be blocked and presumably also the nano-particles can be covered with multiple layers of carbon.

SXRD is also very suitable for studying catalytic surfaces, under realistic conditions, since the interaction between X-rays and gases is very weak. The technique provides structural information about symmetrical surface geometries on a catalyst. This can be linked to reactivity if residual gas analysis is performed simultaneously. A dedicated instrument for this type of in situ study of catalyst surfaces has been developed, and is discussed in detail in [52]. With this technique, nano-particles on a flat support can be studied, as long as the surface is reflective for the X-rays.

Scanning tunnelling microscopy is a suitable technique for bridging the pressure gap, since it is operable under UHV and high pressure conditions, as well as for temperatures ranging from 4 K to >1000 K [56]. This type of microscope can provide real space, atomically resolved, images of the catalytic surface, opening the possibility of studying the surface structure under the influence of different gas environments, of indicating active sites, and studying the role of possible promoters. In addition, the STM has a weak and local interaction with the surface, and will therefore not influence the properties of

[1] Micro-Electro Mechanical Systems

the catalyst. The difficulties of this technique lie in the fact that everything has to be kept small. It also needs a stable environment, in which drift, due to temperature differences, and noise, due to mechanical and acoustical vibrations, have to be kept to a minimum. Additionally, only conducting surfaces can be investigated, which excludes oxide-supported nano-particles.

Atomic force microscopy falls into the same category as STM, but since its operational principle is based on the repulsive force between sample and a cantilever, insulating surfaces can also be studied. This opens the way to studying catalytic nano-particles supported by non-insulating materials. A high-pressure ReactorAFM is in development [55].

Although all the techniques described in this section already approach the realistic working conditions of a catalyst, they all have their limitations, either in sensitivity towards some aspects of the structure or reactivity of a catalyst, or in only partially bridging the materials and/or pressure gaps, depending on which sample and environmental specifications are demanded by the specific technique. Eventually we want to be able to study alloys, nano-particles on porous materials, and catalytically active materials in combination with promoters. Some of the surface sensitive techniques certainly have the potential to be developed in that direction.

1.2 Crystallography

To describe the structure of a crystal, which consists of regularly ordered atoms, a unit cell is defined, after choosing a set of coordinate axes and an origin. This unit cell is spanned by three lattice vectors **a**, **b**, and **c**, with lengths u, v, and w, and mutual angles α, β, and γ. The concept of a unit cell is illustrated in figure 1.3. Figure 1.3 A shows a conventional unit cell for a face-centered cubic crystal[2], defined by $\mathbf{r} = u\mathbf{a} + v\mathbf{b} + w\mathbf{c}$. One of the angles between the vectors is indicated by ϕ; in this case, $\alpha = \beta = \gamma = 90°$. The properties of a unit cell are that it be translationally invariant, and that it should contain all the information necessary to build up the bulk crystal lattice, as shown in figure 1.3 B and C. By translating the unit cell a unit of distance along each of the lattice vectors, it will always place itself in a position equivalent to the position at the origin. The smallest possible unit cell, which still holds all the crystal's information, is called the primitive unit

[2]The different types of crystal structures will be discussed below; I have chosen the face-centered cubic crystal lattice as an example in this section because all the crystals used in this research exhibit the face-centered cubic structure.

cell. This is different from the conventional unit cell. The geometry of the primitive unit cell can be complicated, which makes the use of the conventional unit cell preferable.

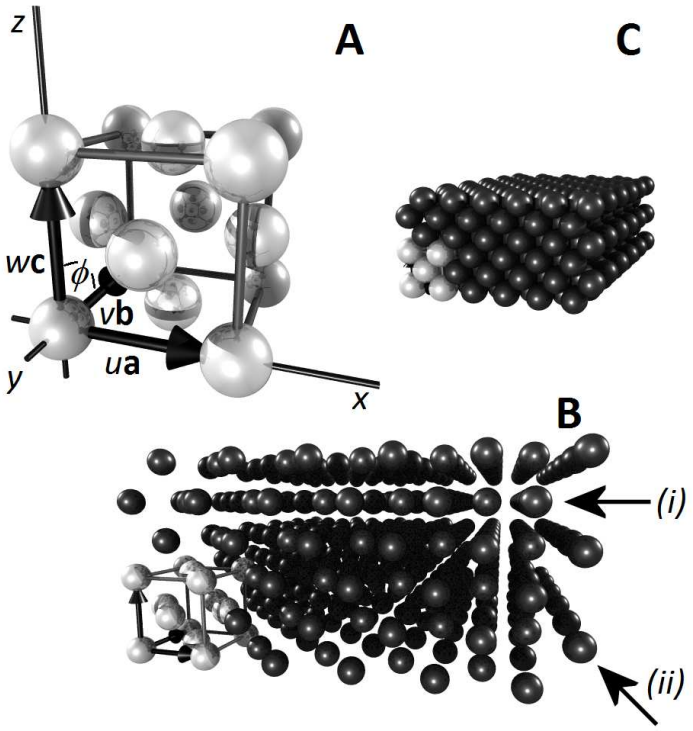

Figure 1.3: Example of a unit cell: the face-centered cubic crystal. (A) Unit cell with lattice vectors $u\mathbf{a}$, $v\mathbf{b}$ and $w\mathbf{c}$; one angle ϕ is indicated. (B, C) The unit cell projected in the bulk crystal lattice.

Looking at figure 1.3 B, one can easily see that it is possible to define sets of equally spaced parallel planes, in different directions through the crystal, two of which are indicated by arrows (i) and (ii). These planes have identical atomic densities. A crystal can be cut and polished along one of these planes, which creates a surface with a specific atomic arrangement and geometry[3]. Different surfaces have different properties; in catalysis, for example, a different surface geometry will provide different adsorption sites and energies, which can influence the reaction rate or selectivity towards a chemical reaction strongly. To name and group all possible plane orientations, Miller

[3]As an example: the various facets on a polished gem, like a diamond, can be grouped according to such planes

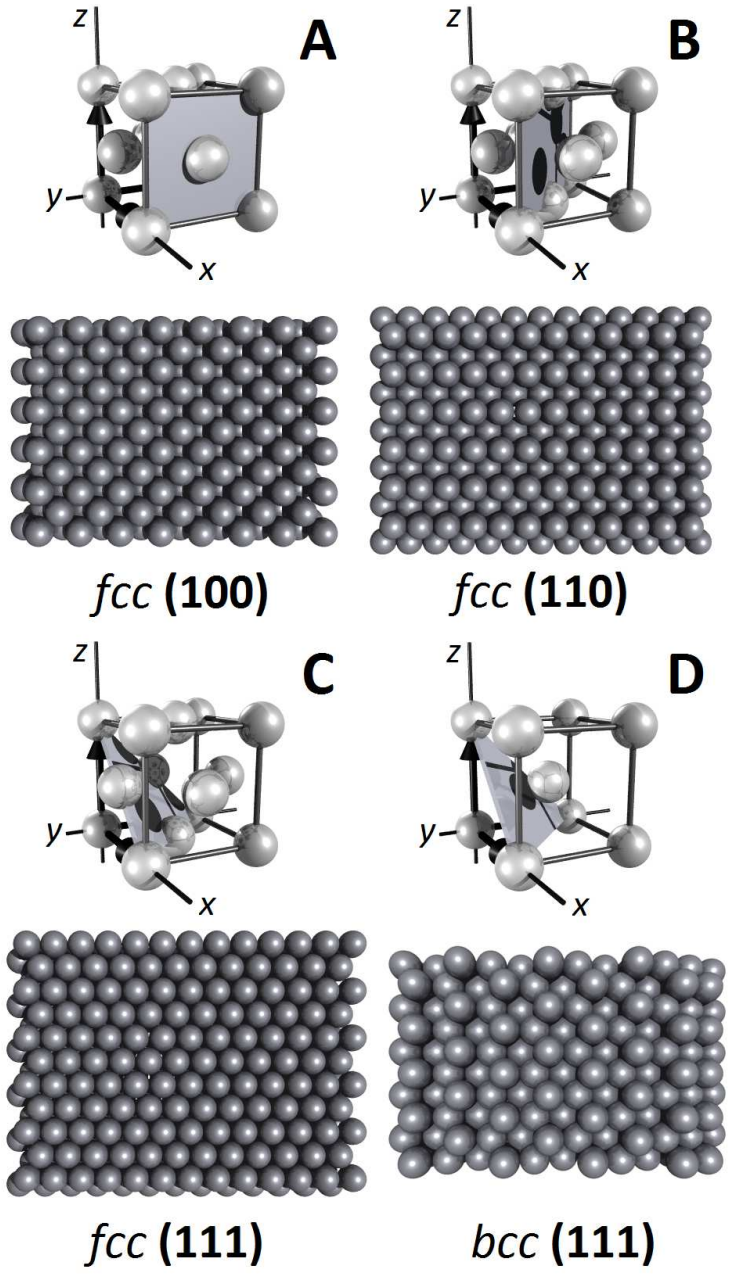

Figure 1.4: (A) The face-centered cubic unit cell, in which the (100) Miller index plane is shown (top), with corresponding surface termination (bottom). (B) The (110) Miller index plane and surface. (C) The (111) Miller index plane and surface. (D) The (111) Miller index plane and surface for the body-centered cubic lattice.

indices were introduced, which are defined as intercepts of the (Miller) plane on the crystal axes closest to the origin, and therefor consist of three digits. As an example, figure 1.4 shows three different geometries for such a plane for the face-centered cubic lattice, in combination with the corresponding surface termination. The top part of figure 1.4 A shows the (100) plane for the crystal: the plane cuts through the x-axis at $x = 1$, and runs parallel along the y and z-axis, hence (100). The bottom part shows the geometry of the surface when a crystal is cleaved along this direction. Similarly, figure 1.4 B shows the (110) plane, and figure 1.4 C the (111) plane. As can be seen, the surface termination of a crystal varies strongly with the orientation of the Miller plane. Polishing a crystal along higher Miller index planes, e.g. (553), creates stepped and vicinal surfaces [37].

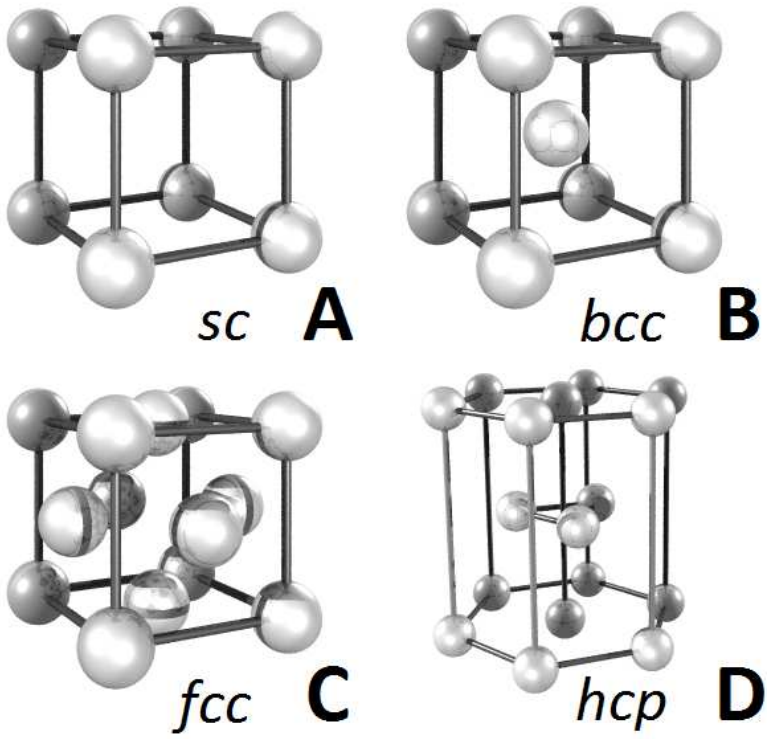

Figure 1.5: (A) The simple cubic lattice, (B) the body-centered cubic lattice, (C) the face-centered cubic lattice, and (D) the hexagonal close-packed lattice

In figure 1.3 and 1.4, the face-centered cubic crystal structure is used as an example. More structures exist, of which the conventional unit cells of the most common ones are illustrated in figure 1.5 – nearly all metals have

one of these structures. The first structure shown is the simple cubic lattice (sc), in which the unit cell contains exactly one atom. Polonium is reported to have this structure. The unit cell of the body-centered cubic (bcc) structure, containing two atoms, is shown in figure 1.5 B. Examples of metals having this crystal structure are iron, tungsten, and sodium. And finally, the face-centered cubic (fcc) structure, is depicted in figure 1.5 C. This unit cell contains four atoms, and exhibits the closest possible packing for cubic lattices. Nickel, silver, and gold are examples of metals with this structure. In addition to cubic stacking, there is also the possibility of stacking the atoms hexagonally, which is shown in figure 1.5 D. This is called the hexagonal close-packed (hcp) structure. Examples are zinc, titanium, and cobalt [38]. The crystal structure also influences the surface termination, which is illustrated in figures 1.4 C and D; both show a (111) Miller index plane. In figure 1.4 C, the (111) plane is for an fcc lattice, and in figure 1.4 D, the (111) plane for a bcc lattice.

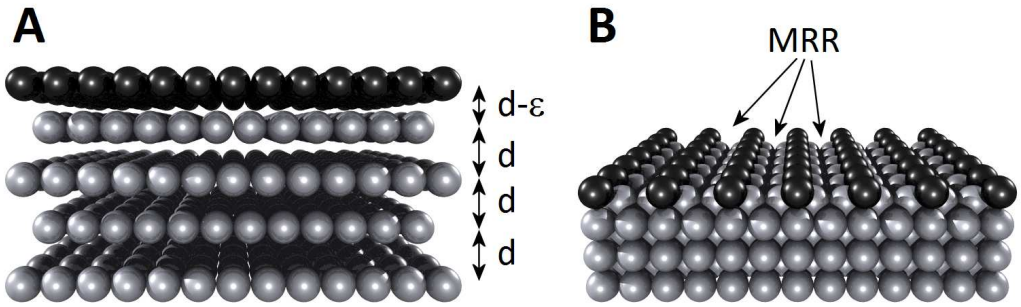

Figure 1.6: Examples of surface relaxation and reconstruction, using the fcc (110) surface. (A) Relaxation: the distance between the surface layer and the layer below is contracted by ϵ with respect to the bulk distance d. (B) Reconstruction: the surface layer termination is different from the bulk crystal. In the fcc (110) lattice, every second row of atoms on the surface is missing, creating the so-called missing-row reconstruction (MRR).

In the bulk of a crystal, the forces exerted on the equilibrium positions of the individual atoms by their surroundings are equal. At the surface, however, these forces change, which can lead to relaxation or reconstruction of the atoms at the surface. When the surface undergoes relaxation, the entire surface shifts with respect to the bulk, without changing the other interatomic distances at the surface. Since there is an attractive force towards the bulk, relaxation often induces the top layer to decrease its distance to the bulk, resulting in a different inter-layer distance than that within the

bulk itself (fig. 1.6 A). This type of relaxation is common for most metals. Reconstruction, on the other hand, also includes rearrangement of atoms on the surface layer, resulting in a different surface geometry, with respect to the bulk [39]. This happens, for instance, at the lower Miller index planes of the late 5d metals gold, iridium, and platinum, due to a significantly larger tensile surface stress in these metals than in the related 3d and 4d metals. This causes the 5d metals to reconstruct, rather than just to relax. It is believed that, next to the electron density within the 5d metals, the stronger bonding of low coordination atoms is caused by competition between the s and d electrons, arising from relativistic effects [40–42]. The surface reconstructions occurring are, for instance, hexagonal close packing on the (111) surface, a missing-row reconstruction on the (110) surface (fig. 1.6 B), and a quasi-hexagonal restructuring of the (100) surface. Due to the difference in symmetry between the unreconstructed and reconstructed lattices, the periodicity of these surface structures is usually quite large; typical commensurate unit cells are (1x5) or (5x20) [43].

When two similar grids are overlayed at an angle, or when two slightly different grids are overlayed, an interference pattern is created, called a Moiré pattern. The effect is illustrated in figure 1.7. When the two grids are rotated with respect to each other, the interference pattern can clearly be seen as a recurring structure, with a larger periodicity than the separate grids (B), whereas it cannot be observed when they overlay at the same angle (A) [44].

This phenomenon also occurs on the atomic scale, for instance when the surface of a crystal has a different orientation or structure, with respect to the bulk, as in the case for the surface reconstructions just discussed[4], or when two different materials are superimposed on each other, which have the same lattice structure, but different interatomic spacing[5]. The patterning effect can be observed by a scanning tunneling microscope. When the surface is only liable to relaxation, which would be similar to the situation in figure 1.7 A, no pattern formation will occur.

[4]This is the case for Pt(100), which we have used for NO reduction in chapter 3

[5]This happens when MoS_2 is evaporated onto Au(111), which is discussed in chapter 5

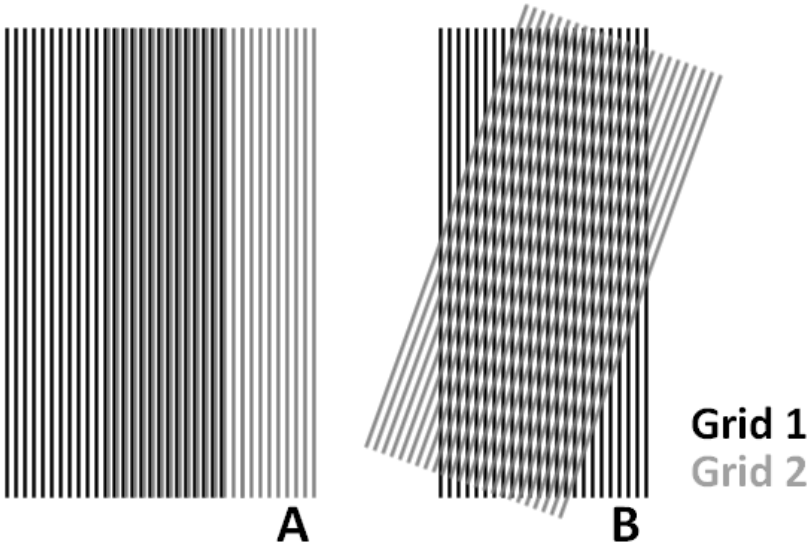

Figure 1.7: (A) Two grids overlayed at the same angle exhibit no interference pattern. (B) When rotated with respect to each other, an interference pattern can be observed, superimposed on the two grids

1.3 Scanning Tunneling Microscopy

1.3.1 STM in general

The concept of scanning tunneling microscopy was invented in 1981 by Binnig and Rohrer [10], for which they were awarded the Nobel Prize in physics in 1986. The technique enabled both high resolution imaging and manipulation of individual atoms on conducting surfaces, routinely. The basic elements of an STM are shown in figure 1.8.

A sharp tip, usually made out of chemically etched tungsten or mechanically sheared platinum iridium, and a conducting sample are brought together, to within a few atomic distances ($\sim$5 Å) of each other, such that the electron wave functions of sample and tip overlap. If, in this situation, a bias voltage V_b is applied between the tip and the sample, quantum mechanics predicts that there is a nonzero probability for electrons to tunnel through the vacuum barrier. This yields an electrical current between tip and sample, the tunneling current I_t (eqn. 1.3.1). This current depends exponentially on the distance between tip and sample d, which leads to the extremely high resolution of the STM: when the distance between tip and sample is increased by 1 Å, the tunneling current decreases one order of magnitude [11, 12].

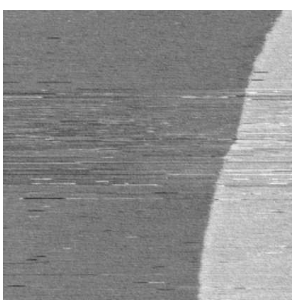

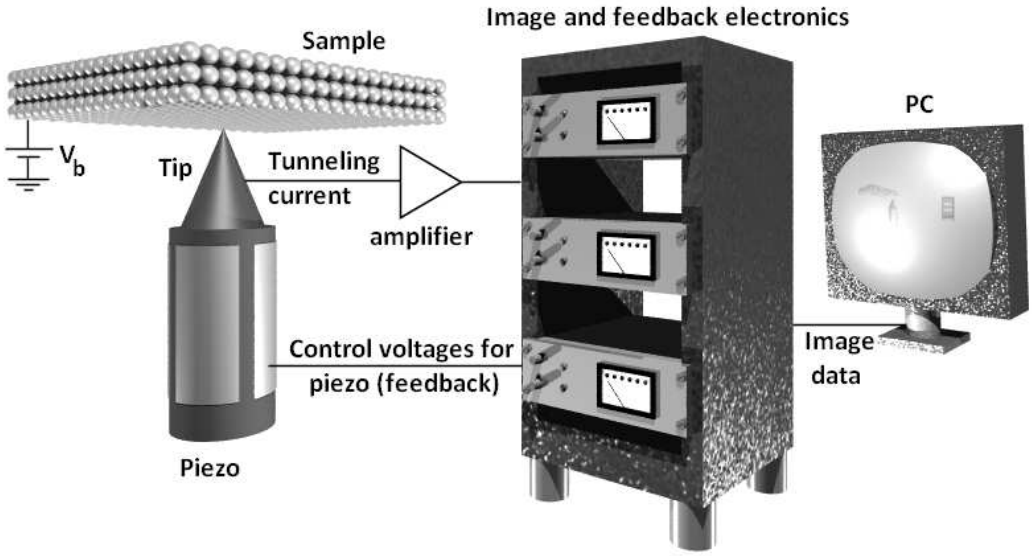

Figure 1.8: The concept of a scanning tunneling microscope

$$I_t \propto V_b \exp\left(-2\sqrt{\frac{2m\Phi}{\hbar^2}}\, d\right). \tag{1.3.1}$$

The usual modus operandi of an STM is raster-scanning the tip across the surface, while the tunneling current is monitored at a fixed bias voltage. The motion of the tip in x, y, and z is controlled by a piezo[6] tube, containing separate piezoelectric elements for each direction. By applying a sawtooth voltage to the x piezo and a voltage ramp on the y piezo, the raster-scanning motion can be generated. During scanning, a feedback circuit can regulate the STM in two modes: the constant current mode and the constant height mode. In the constant current mode, the feedback circuit regulates the voltage on the z-piezo to adjust the distance between tip and sample, maintaining a constant tunneling current during scanning motion. The feedback signal, which is directly related to the z position of the tip and stored as a function of the x and y position, translates into a topographical image on the computer screen. In constant height mode, the z position of the piezo is kept constant. In this way the tunneling current can be directly correlated to surface structure, which as a function of x and y translates again into a topographical image. The choice between the two feedback modes is determined by the target of the research: the constant current mode provides higher image res-

[6]A piezoelectric material is a material that contracts or expands under the influence of an applied voltage.

olution, whereas the constant height mode enables faster data acquisition. To gain high resolution with an STM, it is important to make the system as insensitive to vibrations as possible. This can be achieved by, on the one hand, constructing the STM to be as rigid as possible, and, on the other hand, by using active and passive damping systems, such as, for instance, an Eddy-current damping mechanism for damping external mechanical and acoustic vibrations [11, 13].

STM is a very powerful technique, as it can be operated in very diverse environments: under ultrahigh vacuum and high pressure environments, low (mK range) and high (10^3 K range) temperature environments, and in various liquid environments. The fields in which STM is being used include thin film growth [14–16], self assembled monolayers [17–19], electro chemistry [20–22], and catalysis [12, 23, 27].

1.3.2 ReactorSTM^{TM}

ReactorSTM^{TM}: The concept

In figure 1.9, a conceptual drawing of the ReactorSTM^{TM} is presented. Given is a reactor volume V, with inert walls, to which two thin gas lines are connected: (1) gas inlet and (2) gas outlet. The inlet is connected to a gas system, which can mix gases A and B in a chosen ratio to flow this into the reactor volume. The outlet leads to a quadrupole mass spectrometer, for residual gas analysis of the exhaust. Only the STM tip is exposed to the reactor volume: a ring R_1 separates the rest of the approach motor from the reactor volume. In this way, the reactor volume is kept small, to enhance refresh rate and response time, and so that the different elements of the approach motor are not exposed to high pressures of violent gases. A ring R_2, on which the sample is pressed, seals the reactor volume from the UHV environment surrounding it. Along these lines, the sample surface, which can be heated from the back, is exposed to the high gas pressures, and can be approached by the tip.

ReactorSTM^{TM}: The setups

The work in this thesis has been performed in two different ReactorSTM's, which will be distinguished by adding "Mark I" or "Mark II" to the name. ReactorSTM Mark I was developed approximately a decennium ago and is briefly described in this section. An in depth description of this microscope

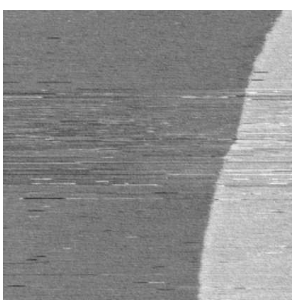

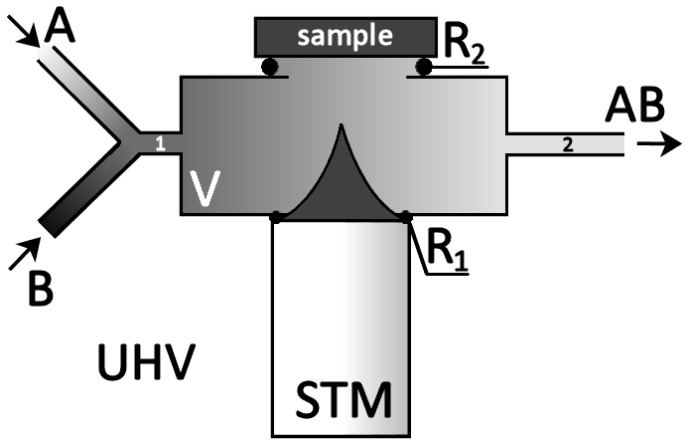

Figure 1.9: Conceptual drawing of the STM. (V) Reactor volume, (A), (B), (AB) gases, (R_i) flexible rings.

can be found in [53]. Chapter 2 is fully dedicated to the newly designed ReactorSTM Mark II; its development was part of the work described in this thesis.

The experiments described in chapter 3 and part of the experiments described in chapter 5 of this thesis have been carried out in the ReactorSTM Mark I. A 3D impression of the vacuum system in which it is housed, in combination with a technical drawing of the STM itself, is shown in figure 1.10.

With the ReactorSTM^{TM}, model catalyst surfaces can be imaged at elevated temperatures and atmospheric pressures [27, 53]. The instrument features an STM integrated with a small (0.5 ml) flow reactor cell (1), through which a variety of clean gas mixtures can be allowed to flow, at pressures up to 2 bar. The construction of the STM-reactor combination is such that only the STM-tip and its holder (2) are inside the reactor, while the other STM components, such as the piezo element (3), are outside. The entire ReactorSTM^{TM} system is housed in an ultrahigh vacuum (UHV) chamber (4). This enables us to prepare and characterize the sample surface by state-of-the-art surface-science techniques (see below). After preparation, the sample (5) is pressed firmly against the flow reactor. In that geometry, it forms one of the walls of the reactor. A Kalrez ring, between the sample and the rest of the reactor serves as a nearly UHV-tight seal between the reactor volume and the vacuum chamber (6). In order to measure the gas composition inside the reactor, and thus derive the catalytic conversion rates, we take

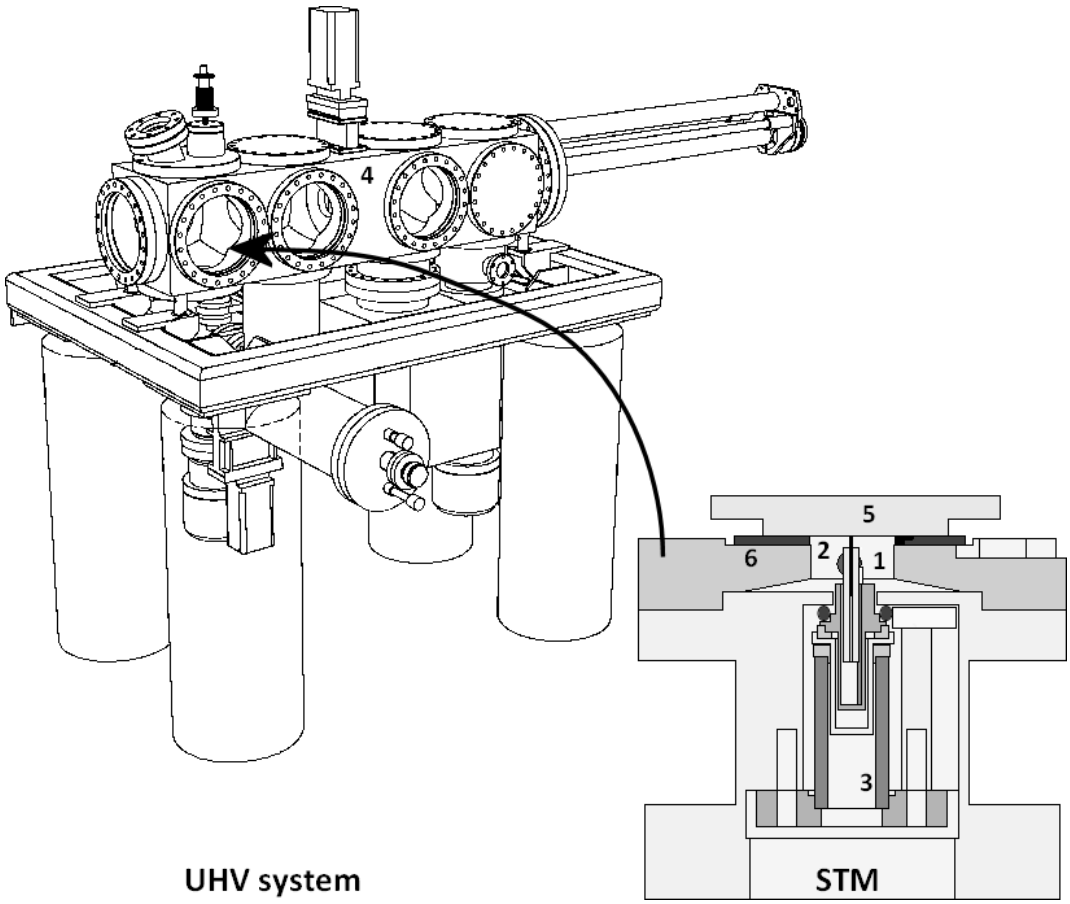

Figure 1.10: The UHV system and cross-section of the ReactorSTM Mark I.

advantage of the small gas leak over the Kalrez seal into the UHV chamber, which is equipped with a quadrupole mass spectrometer (QMS). The sample holder contains a filament, located directly behind the model catalyst. With this, the sample can be heated, both for preparation purposes and during actual experiments, when the sample is placed on the reactor.

The flow, pressure, and composition of the gas mixtures are controlled by a gas system combining a series of mass flow controllers before the reactor, one for each high-purity gas, and a back-pressure controller behind the reactor. This configuration allows us to vary the composition without changing total pressure. In our experiments, the total pressure was fixed at 1.25 bar and the flow rate was set to 8 ml_n per minute, corresponding to a refresh time of the reactor volume of 4 sec.